Articles

Phase Properties of Carbon-Supported Gold−Platinum Nanoparticles with Different Bimetallic Compositions

Jin Luo,† Mathew M. Maye,† Valeri Petkov,‡ Nancy N. Kariuki,† Lingyan Wang,† Peter Njoki,† Derrick Mott,† Yan Lin,† and Chuan-Jian Zhong*,†

Department of Chemistry, State University of New York at Binghamton, Binghamton, New York 13902, and Department of Physics, Central Michigan University, Mt. Pleasant, Michigan 48859

Received January 10, 2005. Revised Manuscript Received March 10, 2005

The ability to control the composition and phase properties of bimetallic nanoparticles is critical in exploring catalytic properties. In this paper we present results from a study aimed at determining those properties for carbon-supported gold−platinum (AuPt) catalysts with different bimetallic compositions. The bimetallic nanoparticle catalysts are prepared by a two-phase synthesis protocol employing organic monolayer encapsulation on bimetallic AuPt cores (∼2 nm). The size-controlled nanoparticles are assembled on carbon black support materials with controllable dispersion and metal loading and are further treated by calcination under controlled temperature and atmosphere. The core composition of the bimetallic nanoparticles is determined by direct current plasma-atomic emission spectroscopy. Structural characterization is carried out by X-ray diffraction. The bimetallic nanoparticles were shown to display alloy properties, which is in sharp contrast to the bimetallic miscibility gap known for the bulk counterpart of the bimetallic metals. This finding demonstrates the difference of the physical and chemical properties for nanoscale materials from the bulk crystalline state, revealing important details of the phase properties of the bimetallic nanoparticle catalysts and new information for the correlation between the composition and the phase properties at the nanoscale. Implications of our findings to the design and manipulation of the bimetallic nanoparticles for catalytic applications are also discussed.

Introduction

Binary PtRu nanoparticles have for a long time been one of the most-studied catalyst systems[1,2] because of their bifunctional catalytic properties. For example, in catalytic oxidation reaction of methanol, Pt provides the main site for the dehydrogenation of methanol and Ru provides the site for hydroxide (OH) for the oxidation of CO-like species to CO_2. Recently, gold nanoparticles were found to show unprecedented catalytic activities for CO oxidation[3−11] and electrocatalytic activity for CO and methanol oxidation.[12−15] For methanol oxidation reaction (MOR) at the anode in methanol oxidation fuel cells, gold-based bimetallic materials could potentially provide a synergistic catalytic effect. For example, gold−platinum (AuPt) nanoparticles could help both suppress adsorbed poisonous species and modify the strength of the surface adsorption. This may be achieved by having Pt-based surface sites function as main hydrogenation or dehydrogenation sites while the synergistic effect of Au and Pt is to speed up the removal of the poisonous species. Mechanisms such as decreasing the activation energy of oxidative desorption and suppressing the adsorption of CO were previously considered to result in an adsorptivity high enough to support catalytic oxidation in alkaline electrolytes.[16−19]

* To whom correspondence should be addressed. E-mail: cjzhong@binghamton.edu.
† State University of New York at Binghamton.
‡ Central Michigan University.

(1) Reddington, E.; Sapienza, A.; Gurau, B.; Viswanathan, R.; Sarangapani, S.; Smotkin, E. S.; Mallouk, T. E. *Science* **1998**, *280*, 1735.
(2) Liu, R. X.; Smotkin, E. S. *J. Electroanal. Chem.* **2002**, *535*, 49.
(3) Haruta, M. *Catal. Today* **1997**, *36*, 153.
(4) Haruta, M.; Date, M. *Appl. Catal. A* **2001**, *222*, 427.
(5) Bond, G. C.; Thompson, D. T. *Gold Bull.* **2000**, *33*, 41.
(6) Corti, C. W.; Holliday, R. J.; Thompson, D. T. *Gold Bull.* **2002**, *35*, 111.
(7) *Gold 2003−New Industrial Applications for Gold, Proceeding Volume*; World Gold Council: Vancouver, 2003.
(8) Valden, M.; Lai, X.; Goodman, D. W. *Science* **1998**, *281*, 1647.
(9) Cameron, D.; Holliday, R.; Thompson, D. *J. Power Sources* **2003**, *118*, 298.
(10) Rolison, D. R. *Science* **2003**, *299*, 1698.
(11) Jaramillo, T. F.; Baeck, S. H.; Cuenya, B. R.; McFarland, E. W. *J. Am. Chem. Soc.* **2003**, *125*, 7148.
(12) Zhong, C. J.; Maye, M. M.; Luo, J.; Han, L.; Kariuki, N. N. In *Nanoparticles: Building Blocks for Nanotechnology*; Rotello, V. M., Ed.; Kluwer Academic Publishers: New York, 2004; Chapter 5, pp 113−144.
(13) Zhong, C. J.; Luo, J.; Maye, M. M.; Han, L.; Kariuki, N. N. In *Nanotechnology in Catalysis*; Zhou, B., Hermans, S., Somorjai, G. A., Eds.; Kluwer Academic/Plenum Publishers: New York, 2004; Vol. 1., Chapter 11, pp 222−248.
(14) Zhong, C. J.; Maye, M. M. *Adv. Mater.* **2001**, *13*, 1507.
(15) Luo, J.; Maye, M. M.; Kariuki, N. N.; Wang, L.; Njoki, P.; Han, L.; Schadt, M.; Lin, Y.; Naslund, H. R.; Zhong, C. J. *Catal. Today* **2005**, *99*, 291.
(16) Nishimura, K.; Kunimatsu, K.; Enyo, M. *J. Electroanal. Chem.* **1989**, *260*, 167.

10.1021/cm050052t CCC: $30.25
Published on Web 05/11/2005

A recent study showed[20] that catalysts prepared from Pt and Au precursors by impregnation are similar to those of monometallic Pt catalysts, suggesting that the presence of Au did not affect the catalytic performance of Pt in any significant way. This was attributed to a phase segregation of the two metals due to their miscibility gap.[21] As a result, only Pt participates in the adsorption of CO and the catalytic reaction. How the bimetallic catalytic properties depend on nanoparticle preparation and composition is an important question that must be answered for the development of bimetallic catalysts with new or improved properties. To our knowledge, little has been reported about the phase properties of the AuPt bimetallic nanoparticles with different compositions.

In this paper, we report the results from a study of the morphological and phase properties of carbon-supported gold−platinum catalysts with different bimetallic compositions. The bimetallic nanoparticle catalysts are prepared by two-phase synthesis with organic monolayer encapsulation on the nanocrystal core, followed by an assembly on carbon black support materials and thermal calcination. The bimetallic compositions are determined by direct current plasma-atomic emission spectrometry (DCP-AES), and the crystalline and phase properties are characterized by X-ray diffraction (XRD). The AuPt nanoparticles prepared in this way are found to exhibit alloy properties in sharp contrast to the bimetallic miscibility gap known for the bulk counterparts of AuPt metals.

Experimental Section

Chemicals. Decanethiol (DT, 96%), hydrogen tetrachloroaurate ($HAuCl_4$, 99%), tetraoctylammonium bromide (TOABr, 99%), hydrogen hexachloroplatinate (IV) ($H_2PtCl_6 \cdot xH_2O$, 99.995%), sodium borohydride ($NaBH_4$, 99%), and oleylamine (OAM, 70%) were purchased from Aldrich and used as received. Other chemicals included hexane (99.9%) and toluene (99.8%) from Fisher and methanol (99.9%) and ethanol (99.9%) from Aldrich. The catalyst of Pt/C (20% Pt on Vulcan XC-72) was purchased from E-Tek.

Preparation. Gold (Au) and gold−platinum (AuPt) nanoparticles of 2-nm core size encapsulated with an alkanethiolate monolayer shell were synthesized by a modified two-phase method.[22−24] Briefly $AuCl_4^-$ and $PtCl_6^{2-}$ were first transferred from aqueous solution of $HAuCl_4$ and H_2PtCl_6 into toluene solution using a phase-transfer reagent (tetraoctylammonium bromide). Thiols (e.g., decanethiol, DT) or amine compounds (e.g., oleylamine, OAM) were added to the organic solution as capping agents. An excess of aqueous $NaBH_4$ was slowly added for the reduction reaction. The resulting DT/OAM-encapsulated AuPt nanoparticles in toluene were collected by removing the solvent and cleaned using ethanol. The nanoparticle product was dissolved in hexane. The bimetallic composition of the AuPt nanoparticles was determined by DCP-AES.

Carbon black XR-72C obtained from Cabot was used as support materials. The carbon black was first pretreated by suspending in hexane and sonicated for ~6 h at room temperature. A controlled amount of AuPt nanoparticles was added into the suspension. The suspension was sonicated for 30 min, followed by stirring overnight. Thus-prepared carbon-supported AuPt powders were collected and dried under N_2. The loading of AuPt on the carbon support was controlled by monitoring the weight ratio of AuPt nanoparticles vs carbon black. The actual loading was determined by thermogravimetric analysis (TGA) and DCP-AES analysis.

Treatment. The carbon-loaded nanoparticles were treated in a tube furnace under controlled temperature and atmosphere. A typical calcination protocol included shell removal by annealing at 300 °C under 20% O_2/N_2 for 1 h and calcination at 400 or 500 °C under 15% H_2/N_2 for 2 h. The carbon-loaded Au or AuPt nanoparticles are denoted as Au/C or AuPt/C. It is important to note that while this treatment condition was found to produce very active catalysts, poor catalytic activities were occasionally observed for some catalysts, which we believe was likely due to burning of the carbon support materials catalyzed by the highly active bimetallic nanoparticle catalysts. The origin of the "burning effect" is not completely clear at this point.

Instrumentation and Measurement. *Direct Current Plasma-Atomic Emission Spectroscopy (DCP-AES).* The nanoparticle composition was analyzed by direct current plasma-atomic emission spectroscopy on an ARL Fisons SS-7 direct current plasma-atomic emission spectrometer. Measurements were made on emission peaks at 267.59 and 265.95 nm for Au and Pt, respectively. The nanoparticle samples were dissolved in concentrated aqua regia and then diluted to concentrations in the range of 1−50 ppm for the analysis. Calibration curves were made using dissolved standards with concentrations from 0 to 50 ppm in the same acid matrix as the unknowns. Detection limits, based on three standard deviations of the background intensity, are 0.008 and 0.02 ppm for Au and Pt, respectively. Standards and unknowns were analyzed 10 times each for 3 s counts. Instrument reproducibility, for concentrations greater than 100 times the detection limit, results in less than ±2% error.

Transmission Electron Microscopy (TEM). TEM was performed on an Hitachi H-7000 electron microscope (100 kV). For the TEM measurement, AuPt or AuPt/C samples were suspended in hexane solution and were drop cast onto carbon-coated copper grids followed by solvent evaporation in air at room temperature.

X-ray Powder Diffraction (XRD). Powder X-ray diffraction data were collected on a Philips X'Pert diffractometer using Cu Kα radiation ($\lambda = 1.5418$ Å). The measurements were done in reflection geometry and the diffraction (Bragg) angles 2Θ were scanned at a step of 0.025°. Each data point was measured for at least 20 s and several scans were taken on each sample. The scans were combined to reduce the effect of the instrument's instability and improve the statistical accuracy of the diffraction data.

Thermogravimetric Analysis (TGA). To determine the actual loading of metal nanoparticles on the carbon black support, TGA analysis of the catalysts was performed using a Perkin-Elmer Pyris 1 TGA instrument. Typical samples weighed ~4 mg and were heated in a platinum pan under 20% O_2 atmosphere at a rate of 10 °C/min.

Results and Discussion

The experimental results and their discussion are presented in two subsections. In the first section, the size and

(17) Morita, M.; Iwanaga, Y.; Matsuda, Y. *Electrochim. Acta* **1991**, *36*, 947.
(18) Anderson, A. B.; Grantscharova, E.; Seong, S. *J. Electrochem. Soc.* **1996**, *143*, 2075.
(19) Burke, L. D.; Collins, J. A.; Horgan, M. A.; Hurley, L. M.; O'Mullane, A. P. *Electrochim. Acta* **2000**, *45*, 4127.
(20) Mihut, C.; Descorme, C.; Duprez, D.; Amiridis, M. D. *J. Catal.* **2002**, *212*, 125.
(21) *Catalysis by Metals and Alloys*; Ponec, V., Bond, G. C., Eds.; Elsevier: Amsterdam, 1995.
(22) Brust, M.; Walker, M.; Bethell, D.; Schiffrin, D. J.; Whyman, R. *J. Chem. Soc., Chem. Commun.* **1994**, 801.
(23) Hostetler, M. J.; Zhong, C. J.; Yen, B. K. H.; Anderegg, J.; Gross, S. M.; Evans, N. D.; Porter, M. D.; Murray, R. W. *J. Am. Chem. Soc.* **1998**, *120*, 9396.
(24) Maye, M. M.; Kariuki, N. N.; Luo, J.; Han, L.; Njoki, P.; Wang, L.; Lin, Y.; Naslunda, H. R.; Zhong, C. J. *Gold Bull.* **2004**, *37*, 217.

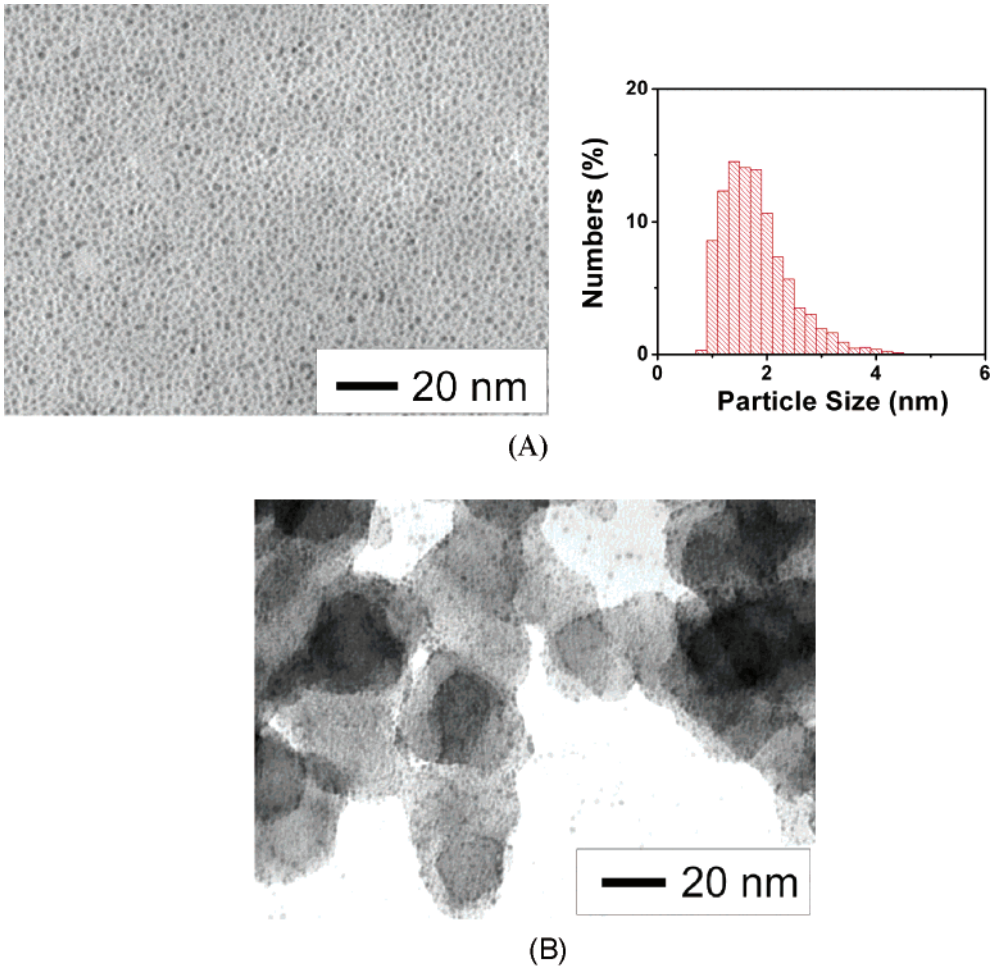

Figure 1. TEM images and particle size distribution for $Au_{82}Pt_{18}$ nanoparticles (A) and $Au_{82}Pt_{18}$/C with 20 wt % metal loading (B).

composition of the Au_mPt_{100-m} (where m represents the relative atomic percentage of Au in the bimetallic nanoparticles) nanoparticles obtained from TEM and DCP-AES experiments are described. In the second, we present the experimental XRD data for the Au_mPt_{100-m}/C catalysts and discuss the phase characteristics and unit cell constants of the nanoparticle catalysts. The outcomes of the discussion provide new information about the correlation between the nanoscale phase property and the bimetallic composition.

1. Size and Composition. DCP-AES analysis of the bimetallic nanoparticles synthesized under the experimental conditions described above showed that the composition of the nanoparticles could be well-controlled. Nanoparticles with different atomic compositions ranging from $m = 10\%$ to $m = 90\%$ Au have been obtained.

Figure 1A shows a representative TEM micrograph and size distribution for $Au_{82}Pt_{18}$ nanoparticles. The particle size distribution was obtained from the TEM image using size-analysis software. The nanoparticles display a relatively high monodispersity (±0.6 nm), with an average size of 1.8 nm (based on a count of 2568 particles). As evidenced by the uniform interparticle spacing, the particles seem to be well-separated from each other due to the presence of the capping organic monolayer. The presence of such a capping layer is supported by FTIR data showing vibrational bands characteristic of the stretching bands of the capping molecules.

The $Au_{82}Pt_{18}$ nanoparticles assembled onto carbon black also show very good dispersion (Figure 1B). The amount of metallic nanoparticles loaded was determined by TGA, which showed ~20 wt%. The metal loading can be easily controlled by adjusting the relative feed ratio of the nanoparticles and the carbon support material.[15,24] Importantly, the average size of the particles shows little change upon loading, suggesting that the capping shells remain intact while interacting with the carbon support.

Our measurements also showed that the dispersion of the $Au_{82}Pt_{18}$ nanoparticles supported on carbon remains relatively high after calcination in the temperature range of 400−500 °C. However, the average size of the particles was found to increase slightly with the calcination temperature (Figure 2). For example, the average size of $Au_{82}Pt_{18}$ nanoparticles increased to 3.3 ±1.1 nm (A) and to 3.9 ±1.1 nm (B) (based on a count of ~200 particles) after treatment at 400 and 500 °C, respectively.

In addition, our previous FTIR and XPS analyses[25] of the nanoparticle samples showed that the removal of the capping shells from the surface of the bimetallic nanocrystalline core was very effective by the calcination treatment. The vibrational bands characteristic of the capping molecules in the C−H stretching region ($\nu_a(CH_3)$: 2955 cm^{-1}; $\nu_s(CH_3)$: 2872

(25) Luo, J.; Maye, M. M.; Han, L.; Kariuki, N. N.; Jones, V. W.; Lin, Y.; Engelhard, M. H.; Zhong, C. J. *Langmuir* **2004**, *20*, 4254.

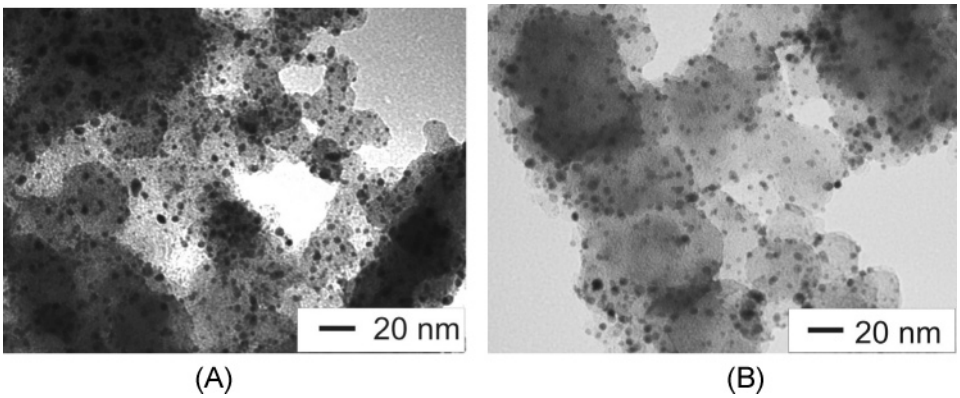

Figure 2. TEM images of $Au_{82}Pt_{18}$/C nanoparticles treated at 400 °C (A) and 500 °C (B).

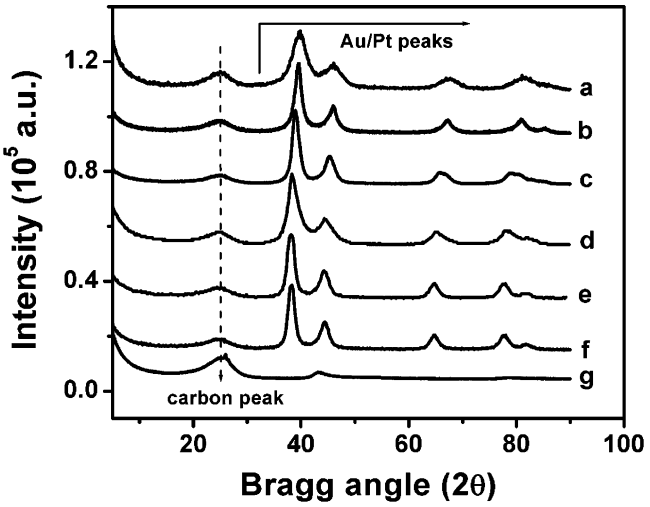

Figure 3. XRD patterns for Pt/C (a), $Au_{35}Pt_{65}$/C (b), $Au_{60}Pt_{40}$/C (c), $Au_{72}Pt_{28}$/C (d), $Au_{82}Pt_{18}$/C (e), Au/C (f) catalysts, and carbon black (g). The chemical composition is determined by DCP-AES. The bimetalic samples are calcinated at 500 °C.

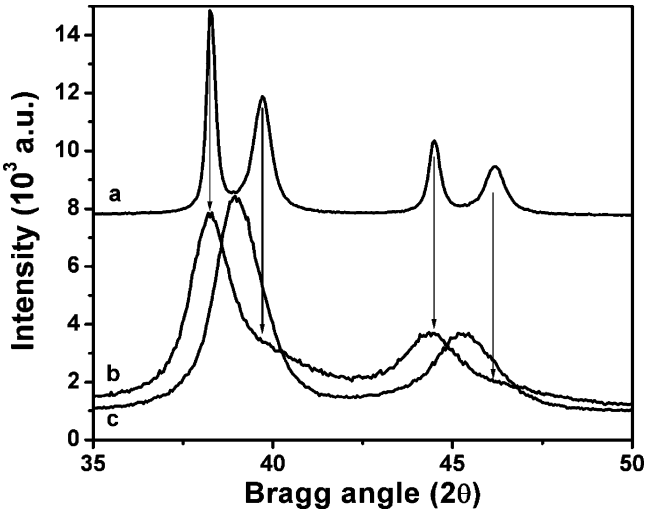

Figure 4. XRD patterns for $Au_{68}Pt_{32}$/C (a) and $Au_{60}Pt_{40}$/C (c) treated at 500 °C. The pattern (b) for a mixture of Au/C and Pt/C is included for comparison. The diffraction peaks originating from the presence of two different nanophases, Au (the lower-angle peak) and Pt (the higher-angle peak), are marked with arrows.

cm^{-1}; $\nu_a(CH_2)$: 2917 cm^{-1}; $\nu_s(CH_2)$: 2848 cm^{-1}) were not detected by FTIR for samples after calcination. XPS analysis of the calcinated samples[25] also showed no bands that can be associated with the presence of sulfur species ($S(2p_{1/2})$ ~ 163.8 eV and $S(2p_{3/2})$ ~ 162.5 eV) on the nanoparticles surface.

2. XRD Characterization. To determine the structural characteristics of the calcinated and carbon-supported bimetallic nanoparticles, we employed X-ray diffraction (XRD). A representative set of XRD data is shown in Figure 3. The XRD patterns for Au/C, Pt/C, and carbon black supporting materials are also included for comparison.

As can be seen in Figure 3, the diffraction patterns for the carbon-supported nanoparticles show a series of broad Bragg peaks, a picture typical for materials of limited structural coherence. Nevertheless, the peaks are defined well enough to allow a definitive phase identification and structural characterization. The diffraction patterns of Au/C and Pt/C could be unambiguously indexed into a fcc-type cubic lattice occurring with bulk gold and platinum. We estimated the corresponding lattice parameters by carefully determining the positions of all Bragg peaks seen in the diffraction patterns. For gold on carbon we obtained a lattice parameter $a = 4.077(2)$ Å, which is practically identical to the literature value of 4.078 Å. Clearly, the Au nanoparticles have the lattice parameter of bulk gold. For platinum on carbon we obtained a lattice parameter $a = 3.927(2)$ Å. It is shorter than the lattice parameter of bulk platinum: $a = 3.97$ Å. It may be due to the fact that Pt/C nanoparticles are rather small (~1−2 nm). For comparison, the average size of Au/C nanoparticles is ~3−4 nm as shown by our TEM analyses. The diffraction patterns of Au_mPt_{100-m}/C nanoparticles also show Bragg peaks that are characteristic of the fcc-type lattice. Moreover, those patterns show a smooth transition from a Au/C-like pattern to a Pt/C-like pattern with the increase of Pt content. This observation indicates that Au_m-Pt_{100-m}/C nanoparticles bear the characteristics of an alloy-type compound involving Au and Pt.

To verify the above assumption, we carefully examined the shape of the Bragg peaks in the diffraction patterns of the Au_mPt_{100-m}/C catalysts. Representative results are shown in Figure 4. One of the diffraction patterns shown (Figure 4a) is from the $Au_{68}Pt_{32}$/C sample which was influenced by the "burning effect" discussed earlier. These nanoparticles are rather large (20−30 nm) and exhibit well-defined Bragg peaks clearly originating from two different phases: nanocrystalline Au (the lower-angle peak) and nanocrystalline Pt

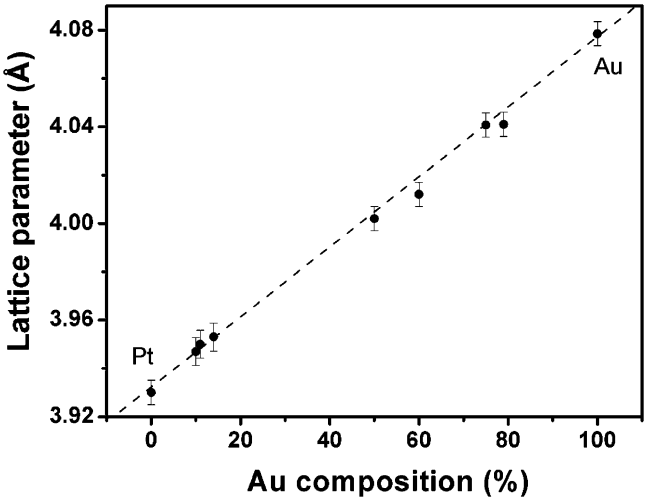

Figure 5. Dependence of the lattice parameters (symbols) for Au_mPt_{100-m}/C nanoparticles on the relative composition of Au%. The broken line is a linear fit to the experimental data.

(the higher-angle peak). The peaks in the diffraction pattern of a physical mixture of Au/C and Pt/C nanoparticles not affected by the "burning effect" (Figure 4b) are rather broad reflecting the small particle size, but highly asymmetric again revealing the presence of two distinct phases. The peaks in the diffraction patterns for the $Au_{60}Pt_{40}$/C catalyst not affected by the "burning effect" (Figure 4c) are also rather broad but fairly symmetric. These peaks fall well between the peaks of Au/C and Pt/C nanophases. The peaks can be perfectly fitted with a single analytical function, suggesting that $Au_{60}Pt_{40}$/C catalyst is indeed a single-phase nanomaterial, i.e., an alloy. Most of the Au_mPt_{100-m}/C catalysts prepared under the experimental conditions described above turned out not to be affected by "burning" of the support and showed diffraction patterns of the type presented in Figure 4c. This observation allowed us to determine the lattice parameters of the corresponding alloys with good accuracy.

The lattice parameters are presented in Figure 5. They were found to scale linearly with the relative Au/Pt content. In other words, they follow a Vegard's type law that is frequently observed with binary metallic alloys.[26] This is an important finding because it shows that the correlation between the phase property and the bimetallic composition for nanoscale materials is different from their bulk counterparts. Bulk Au−Pt metals show a miscibility gap[21] and the linear correlation between the lattice parameter and the composition breaks in a very wide composition range extending from ∼10 to ∼80% Au. Within the miscibility gap, the lattice parameters corresponding to bulk crystalline Au−Pt samples are independent of the composition.

From the observed linear dependence of the lattice parameters on the relative Au/Pt content, we estimated the relative bimetallic composition in the samples. The estimates are presented in Table 1 together with data for Au/Pt composition obtained from the DCP-AES analyses. While the precise values are somewhat different between these two sets of data, the agreement of the general trend between them is quite good, reinforcing our conclusion that the bimetallic Au_mPt_{100-m}/C nanoparticles prepared under the experimental conditions described earlier are indeed alloys. While more closely spaced data points are needed for a better assessment, which is part of our ongoing work, this finding strongly suggests that Au and Pt are likely alloyed in the nanophase state. This finding is again in sharp contrast to the fact that there is a miscibility gap for these two metals in bulk crystalline Au−Pt samples.[21]

Table 1. Comparison of the Bimetallic Composition as Determined by XRD and DCP-AES Experiments

analytical technique	bimetallic composition			
DCP-AES	$Au_{82}Pt_{18}$	$Au_{72}Pt_{28}$	$Au_{60}Pt_{40}$	$Au_{35}Pt_{65}$
XRD	$Au_{80}Pt_{20}$	$Au_{60}Pt_{40}$	$Au_{50}Pt_{50}$	$Au_{17}Pt_{83}$

Using Scherrer's equation relating the coherently scattering domains (L) with Bragg peak widths,

$$L = \frac{k\lambda}{\beta \cos(\theta)}$$

where $k = 0.94$, λ is the wavelength of the radiation used, β is the full-width at half-maximum of the peak in radians, and θ is the Bragg angle, we estimated the average size of the Au_mPt_{100-m}/C nanoparticles studied. The equation was applied to the major (111) peak in the corresponding powder diffraction patterns. The average size of the Au_mPt_{100-m}/C nanoparticles turned out to be ∼4.0 (±0.5) nm, in close agreement with the findings of the TEM experiments. This observation indicated that the nanoparticles are more or less homogeneous at the atomic scale and not partitioned into smaller fragments that are substantially misoriented with respect to one another.

A more detailed study of the atomic ordering in the AuPt/C alloy catalysts, including degree of homogeneity and distribution of Au and Pt on the vertexes of the fcc lattice, would require local probe techniques such as XAFS[27] and atomic pair distribution function analysis.[28,29] Results of such a study will be reported soon.

We further note that the electrocatalytic activities of the calcinated catalysts have been systematically investigated for methanol oxidation reaction[15] and oxygen reduction reaction.[24] The detailed correlation of the results with the nanoscale phase properties will be reported elsewhere.

Conclusion

In conclusion, the bimetallic AuPt nanoparticles prepared by two-phase synthesis, assembly on carbon, and thermal calcination were shown to display alloy properties, which is in sharp contrast to the bimetallic miscibility gap known for the bulk counterpart of the bimetallic AuPt metals. This finding is one of the first examples demonstrating the difference of the physical and chemical properties for nanoscale materials from the bulk crystalline state. A separate

(26) Klug, H. P.; Alexander, L. E. In *X-ray diffraction procedures for polycrystalline and amorphous materials*, second ed.; Wiley: New York, 1974; p 562.

(27) Shibata, T.; Tostmann, H.; Bunker, B.; Henglein, A.; Meisel, D.; Cheong, S.; Boyanov, M. *J. Synchrotron Radiat.* **2001**, *8*, 545.

(28) Petkov, V.; Billinge, S. J. L.; Vogt, T.; Ichimura, A. S.; Dye, J. L. *Phys. Rev. Lett.* **2002**, *89*, 075502.

(29) Petkov, V.; Bozin, E.; Billinge, S. J. L.; Trikalitis, P.; Kanatzidis, M.; Vogt, T. *J. Am. Chem. Soc.* **2002**, *124*, 10157.

ongoing work involves FTIR characterization of the surface bimetallic properties by probing CO adsorption on the catalysts. Further work along this line is in progress to achieve an in-depth understanding of the physics and chemistry of binary or ternary metal materials structured at the nanoscale. Part of our ongoing work also involves the use of HRTEM to characterize the alloy properties. Such understanding will help us gain full control over the bimetallic AuPt nanoparticles with improved catalytic properties.

Acknowledgment. This work was supported in part by the National Science Foundation (CHE 0316322), the Petroleum Research Fund administered by the American Chemical Society (40253-AC5M), and the GROW Program of World Gold Council (RP03-03). The work was also funded in part by NSF under Grant DMR 0304391(NIRT). We also thank Dr. H. R. Naslund (Department of Geological Sciences, SUNY-Binghamton) for assistance in DCP-AES analysis.

CM050052T